IOP Publishing Journal of Physics A: Mathematical and Theoretical
J. Phys. A: Math. Theor. **58** (2025) 035001 (30pp) https://doi.org/10.1088/1751-8121/ada07a

Current fluctuations in finite-sized one-dimensional non-interacting passive and active systems

Arup Biswas[1,2,*], **Stephy Jose**[3], **Arnab Pal**[1,2] and **Kabir Ramola**[3]

[1] The Institute of Mathematical Sciences, CIT Campus, Taramani, Chennai 600113, India
[2] Homi Bhabha National Institute, Training School Complex, Anushakti Nagar, Mumbai 400094, India
[3] Tata Institute of Fundamental Research, Hyderabad 500046, India

E-mail: arupb@imsc.res.in, stephyjose@tifrh.res.in, arnabpal@imsc.res.in and kramola@tifrh.res.in

Received 13 September 2024; revised 29 November 2024
Accepted for publication 17 December 2024
Published 31 December 2024

Abstract
We investigate the problem of effusion of particles initially confined in a finite one-dimensional box of size L. We study both passive as well active scenarios, involving non-interacting diffusive particles and run-and-tumble particles (RTPs), respectively. We derive analytic results for the fluctuations in the number of particles exiting the boundaries of the finite confining box. The statistical properties of this quantity crucially depend on how the system is prepared initially. Two common types of averages employed to understand the impact of initial conditions in stochastic systems are annealed and quenched averages. It is well known that for an infinitely extended system, these different initial conditions produce quantitatively different fluctuations, even in the infinite time limit. We demonstrate explicitly that in finite systems, annealed and quenched fluctuations become equal beyond a system-size dependent timescale, $t \sim L^2$. For diffusing particles, the fluctuations exhibit a $\sqrt{t}$ growth at short times and decay as $1/\sqrt{t}$ for time scales, $t \gg L^2/D$, where D is the diffusion constant. Meanwhile, for RTPs, the fluctuations grow linearly at short times and then decay as $1/\sqrt{t}$ for time scales, $t \gg L^2/D_{\text{eff}}$, where D_{eff} represents the effective diffusive constant for RTPs. To study the effect of confinement in detail, we

* Author to whom any correspondence should be addressed.

also analyze two different setups (i) with one reflecting boundary and (ii) with both boundaries open.

Keywords: statistical physics, active systems, non-equilibrium fluctuations

1. Introduction

The study of the effect of initial conditions on the transport properties of stochastic systems has attracted considerable interest in the past years [1–14]. Notably, these studies have revealed that the distributions of quantities such as the tracer particle displacement or the integrated current across a region are different depending on the initial condition involving the positions of particles [12–15]. Two ensembles of initial conditions that are commonly used to study this effect are (i) annealed setting, which allows for random fluctuations in the initial condition, and (ii) quenched setting, where the initial condition is deterministic [10, 11, 16, 17]. To gain an initial understanding of the relevance of initial conditions, imagine a set of particles initially confined in a one-dimensional channel, free to diffuse. Several intriguing questions arise: Does a static disorder in the initial arrangement of particles influence the dynamic behavior of the system? Furthermore, does this effect persist over large times, particularly when the channel length is finite? What happens if there is an asymmetry in the boundary conditions of this confining channel?

The transport of particles, ions, charges and even living micro-organisms through confined systems remains a topic of interest in various fields such as physics, chemistry and bioengineering with industrial applications [18]. Beginning with Fick [19], and followed by seminal works by Jacobs [20] and Zwanzig [21], the problem of diffusive transport through confined geometries containing narrow openings and bottlenecks has led to many theoretical and experimental research directions. In the context of charge transport through nanopores [22–24], conical tubes [25–27] or membrane channels [28–31] the size of the opening plays an important role in determining the properties of molecular or ionic currents. Additionally from an industrial point of view, filtering of particles using Zeolites [32, 33] or DNA sieving through nanofilter arrays [34] requires explicit knowledge of the length scale associated with the pores. Recently, tabletop experiments have investigated the structure of microfluidic channels of finite length using the escape statistics of colloidal particles diffusing through them [35, 36]. In this context, our work aims to study one such transport quantity, namely the current or flux of non-interacting passive and active particles in a simple one-dimensional confinement setup. Our exact results for these systems explicitly elucidates the role of different initial arrangements of particles on current fluctuations in such confined geometries.

Previous studies have extensively examined the problem of effusion using model systems that are infinitely extended. One such model considers a semi-infinite confining channel bounded between $x \in (-\infty, 0]$, where the fluctuations in the number of particles crossing the origin $x = 0$ up to time t are investigated [14, 37]. For the case of diffusive particles, the annealed setting exhibits larger fluctuations by a factor of $\sqrt{2}$ as compared to the quenched setting [4, 7, 9, 14, 37]. Even for non-interacting active particles, the annealed setting exhibits larger fluctuations by a factor of $\sqrt{2}$ at large times, as the dynamics effectively becomes diffusive [37–39].

More specifically, we focus on the dynamic properties of the particle flux or integrated current Q across the boundaries of a *finite* confining box bounded between $x \in [-L, 0]$. We consider two setups: (i) with a reflecting boundary condition at $-L$, and (ii) with both the boundaries at $-L$ and 0 open. Starting from a random uniform distribution of particles inside the box, we investigate the interplay between these two types of system geometry and two different initial conditions (namely, annealed and quenched initial conditions) on the fluctuations of Q. Interestingly, we demonstrate that in both these cases, annealed and quenched fluctuations converge and become equal at a timescale determined by the system size L and the parameters of the model studied. For diffusing particles, the fluctuations exhibit a $\sqrt{t}$ growth at short times and decay as $1/\sqrt{t}$ for time scales $t \gg L^2/D$, where D represents the diffusion constant. Meanwhile, for run-and-tumble particles (RTPs) [40–50], the fluctuations grow linearly at short times and then decay as $1/\sqrt{t}$ for time scales $t \gg L^2/D_{\text{eff}}$, where D_{eff} denotes the effective diffusive constant for RTPs. For diffusive systems, the ratio of the fluctuations due to annealed and quenched initial conditions changes from a value of $\sqrt{2}$ (which is equal to the ratio observed in an infinite system) at short times to 1 at large times for both the geometries; for active particles, it changes from the value of 2 (infinite system) at short times to 1 at large times in a similar vein. Intriguingly, we also show that the boundary conditions of the confining box play a crucial role in determining the dynamic behavior of Q. The setup with two open boundaries displays larger fluctuations by a factor of 2 at short times and smaller fluctuations by a factor of $1/2$ at large times as compared to the setup with one open boundary for both passive and active cases.

The paper is organized as follows. We provide a simple illustration of different averaging based on the initial conditions in section 2. In section 3, we introduce the models that we use to study the fluctuations in the particle flux Q. In sections 4 and 5, we present exact analytical results for the fluctuations in both diffusive and active systems. We present the conclusions from the study in section 6. Finally, we present details related to some of the calculations in appendices A and B.

2. Quenched versus annealed averages

To illustrate the difference between quenched and annealed averages in stochastic systems, we consider a simple system of a single diffusing particle in one dimension. Let us first examine the quenched scenario. Suppose the particle starts from position x_0 at time $t = 0$. The particle can follow different trajectories (the grey curves), as shown in figure 1(a) (right). The probability distribution of the particle's position will be a Gaussian centered at x_0 with a standard deviation σ_{qu}. That is,

$$P(x, x_0, t) = \frac{1}{\sqrt{4\pi Dt}} \mathrm{e}^{-\frac{(x-x_0)^2}{4Dt}}, \tag{1}$$

where the variance $\sigma_{\text{qu}}^2 = 2Dt$, D being the diffusion constant. Now consider a second case where the particle starts from location x_1 at time $t = 0$ as illustrated in figure 1(a) (left). If we compute the probability distribution, it will again be a Gaussian but centered at x_1 with the same variance σ_{qu}^2. That is,

$$P(x, x_1, t) = \frac{1}{\sqrt{4\pi Dt}} \mathrm{e}^{-\frac{(x-x_1)^2}{4Dt}}. \tag{2}$$

In the quenched case, the cumulants are computed as the average of the cumulants obtained from the different initial realizations. Thus, we obtain the mean and the variance in the quenched case as

$$\langle x \rangle_{\text{qu}} = \frac{x_0 + x_1}{2}, \quad \sigma_{\text{qu}}^2 = 2Dt. \tag{3}$$

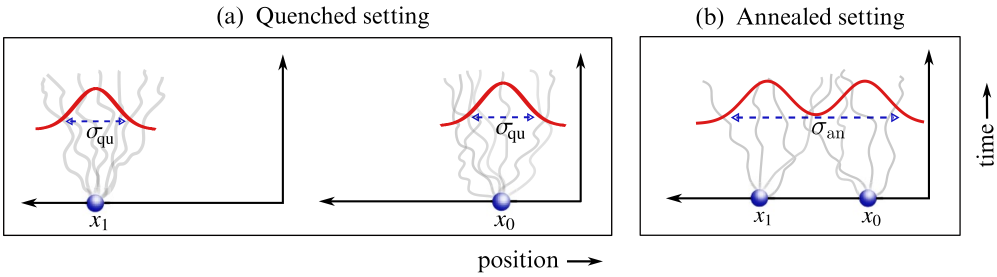

Figure 1. Illustration of (a) quenched and (b) annealed averages for two ($N = 2$) diffusing particles in one dimension. In the quenched setting, the particle starts from a fixed initial position. The occupation probability distribution (red curves) remains the same even if we change the initial position. In the annealed setting, different initial positions are considered simultaneously, and the trajectories (grey curves) obtained from different initial conditions are superposed, yielding a broader distribution indicated by the double-peaked red curve.

Next, we consider the annealed scenario. Here, we consider both initial conditions simultaneously (with equal probability) and superpose the trajectories obtained from both initial conditions as shown in figure 1(b). This will lead to a different probability distribution

$$P(x, x_0, x_1, t) = \frac{1}{4\sqrt{\pi D t}} \left(\mathrm{e}^{-\frac{(x-x_0)^2}{4Dt}} + \mathrm{e}^{-\frac{(x-x_1)^2}{4Dt}} \right). \tag{4}$$

This is the annealed position distribution, and the cumulants are computed with respect to this distribution. This yields the following mean and variance

$$\langle x \rangle_{\rm an} = \frac{x_0 + x_1}{2}, \quad \sigma^2_{\rm an} = 2Dt + \frac{(x_0 - x_1)^2}{4}. \tag{5}$$

We notice that the mean is the same in both the quenched and annealed scenarios. However, the variance is different and is larger in the annealed scenario, as the distribution is broader (as displayed in figure 1). This simple illustrative example demonstrates quenched and annealed averages for a single particle. Usually, these averages are defined for systems with many degrees of freedom with varying timescales for each. The quenched case is usually implemented by fixing some of the slow degrees of freedom and using this as a typical initial condition for the other degrees of freedom. In order to remove the contribution from atypical realizations, we perform an average over the initial conditions. This requires computing the cumulants for each initial condition and then computing their average. In the annealed case, one deals with fast degrees of freedom and the different initial conditions are considered together, requiring a simultaneous averaging of both initial conditions and histories. The history of two ways of averaging (the annealed and the quenched cases) goes all the way to the initial studies by Derrida *et al* [3, 4, 16] followed by an exhaustive list of other studies currently extending to active systems as well.

3. The formalism

In this section, we follow and generalize the formalism developed in [37] to study the fluctuations in the current of particles across the boundaries of a finite-sized box. We consider N

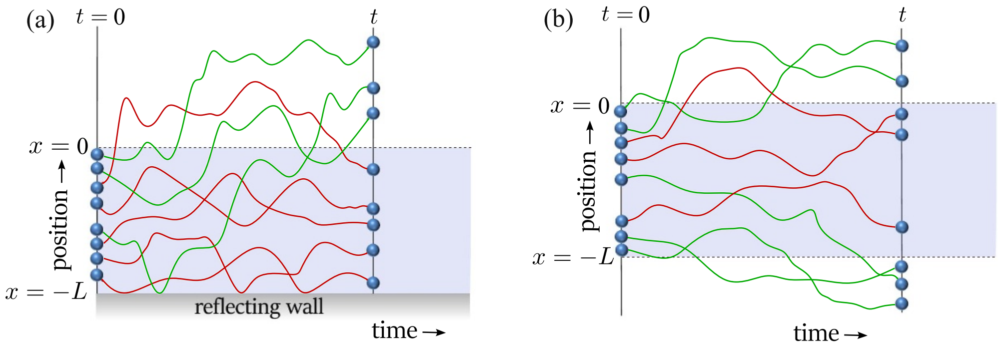

Figure 2. Schematic representation of the trajectories of $N = 8$ non-interacting particles, initially confined in a box bounded between $[-L, 0]$. We are interested in the number of particles present outside this box at time t, denoted as $Q(t)$. The green trajectories indicate those contributing to a non-zero $Q(t)$, while the red ones do not contribute. We examine two setups: (a) in the left panel, a reflecting wall is present at $x = -L$, allowing particles to escape only through the origin $x = 0$. (b) In the right panel, both sides are open, enabling particles to exit through either boundary. In the illustrated figure, $Q(t) = 3$ for the former case and $Q(t) = 5$ for the latter.

non-interacting particles initially distributed with a uniform density $\rho = N/L$ in a finite one-dimensional box bounded between $[-L, 0]$. These particles evolve over time following their underlying dynamics such as diffusion or run-and-tumble motion. The quantity of interest is the number of particles exiting the boundaries of the box up to time t, equivalent to the number of particles present outside the box at time t (see figure 2 for a schematic representation). We denote this quantity as N_t, representing the flux or integrated current through the boundaries of the box up to time t. which can be expressed using an indicator function $\mathcal{I}(t)$, defined as

$$\mathcal{I}_i(t) = \begin{cases} 1, & \text{if the } i\text{th particle is outside } [-L, 0] \text{ at } t, \\ 0, & \text{otherwise.} \end{cases} \tag{6}$$

The quantity N_t is then given as

$$N_t = \sum_{i=1}^{N} \mathcal{I}_i(t) \,. \tag{7}$$

We are primarily interested in the statistical properties of N_t. Generally, two sources of randomness are associated with the measurement of N_t; the randomness in the initial positions of the particles and the randomness due to the inherent stochasticity of the underlying dynamics of the particles. There are two distinct methods for averaging over these sources of randomness: (i) the annealed average—which corresponds to simultaneous averaging over all initial conditions and noise history (ii) the quenched average—where one first averages over noise history for a fixed initial realization, followed by averaging over all possible initial realizations. The formal definitions of these averages are provided in the subsequent sections.

Let us denote by $\{x_i\}$ a distinct set of initial positions of the particles. For the fixed initial positions $\{x_i\}$, the probability distribution of Q is given as

$$P(Q,t,\{x_i\}) = \text{Prob}(N_t = Q) = \left\langle \delta\left(Q - \sum_{i=1}^{N} \mathcal{I}_i(t)\right)\right\rangle_{\{x_i\}}, \tag{8}$$

where $\delta(x)$ is the Dirac-delta function. The angular bracket $\langle\ldots\rangle_{\{x_i\}}$ in the above expression denotes an average over all trajectories of the particles for a fixed initial condition $\{x_i\}$. Moving forward it will be convenient to work with the moment-generating function of Q defined as

$$\begin{aligned}\sum_{Q=0}^{\infty} \mathrm{e}^{-pQ} P(Q,t,\{x_i\}) &= \langle \mathrm{e}^{-pQ}\rangle_{\{x_i\}} \\ &= \left\langle \exp\left(-p\sum_{i=1}^{N} \mathcal{I}_i(t)\right)\right\rangle_{\{x_i\}}.\end{aligned} \tag{9}$$

We next use the identity $\mathrm{e}^{-p\mathcal{I}_i(t)} = 1-(1-\mathrm{e}^{-p})\mathcal{I}_i(t)$ and the independent nature of the dynamics of the particles to obtain

$$\langle \mathrm{e}^{-pQ}\rangle_{\{x_i\}} = \prod_{i=1}^{N} \left[1-\left(1-\mathrm{e}^{-p}\right)\langle \mathcal{I}_i(t)\rangle_{\{x_i\}}\right]. \tag{10}$$

Here $\langle \mathcal{I}_i(t)\rangle_{\{x_i\}}$ represents the probability that the ith particle is present outside the region $x\in[-L,0]$ at time t. Depending on the underlying dynamics and the geometry of the system under consideration, this quantity will be different. We study two different cases where (i) there is a reflecting boundary at $x=-L$ (see figure 2(a)) and (ii) when both the boundaries at $x=0$ and $x=-L$ are open (see figure 2(b)). In the first case, particles exit only through the boundary at $x=0$, however, in the latter case, they exit either through $x=0$ or $x=-L$. Denoting the expectation $\langle \mathcal{I}_i(t)\rangle_{\{x_i\}}$ by $U(x_i,t)$, we obtain

$$U(x_i,t) = \int_0^{\infty} G(x,t|x_i)\,\mathrm{d}x, \tag{11}$$

for the case with a reflecting boundary and

$$U(x_i,t) = \int_{-\infty}^{-L} G(x,t|x_i)\,\mathrm{d}x + \int_0^{\infty} G(x,t|x_i)\,\mathrm{d}x, \tag{12}$$

when both boundaries are open. Here, $G(x,t|x_i)$ is the Green's function defined as the probability density to find a particle at a position x at time t starting from the position x_i at time $t=0$. From equation (10), we obtain the expression for the generating function of Q as

$$\langle \mathrm{e}^{-pQ}\rangle_{\{x_i\}} = \prod_{i=1}^{N} \left[1-\left(1-\mathrm{e}^{-p}\right)U(x_i,t)\right], \tag{13}$$

where the expressions for the function U for the settings with reflecting boundary and open boundaries are given in equations (11) and (12) respectively. The average over the initial conditions $\{x_i\}$ can now be done in two ways, as discussed below.

3.1. Annealed setting

Let us denote by the symbol $\overline{(\ldots)}$ as an average over the initial conditions on the positions of the particles. Performing an average over the initial positions in equation (13), we obtain

$$\overline{\langle e^{-pQ}\rangle_{\{x_i\}}} = \prod_{i=1}^{N}\left[1-\left(1-\mathrm{e}^{-p}\right)\overline{U(x_i,t)}\right]. \tag{14}$$

Since the position of each particle is distributed independently according to a uniform distribution in the interval $x_i \in [-L, 0]$, this expectation can be further simplified to

$$\begin{aligned}\overline{\langle \mathrm{e}^{-pQ}\rangle_{\{x_i\}}} &= \prod_{i=1}^{N}\left[1-\left(1-\mathrm{e}^{-p}\right)\frac{1}{L}\int_{-L}^{0} U(x_i,t)\,\mathrm{d}x_i\right] \\ &= \left[1-\left(1-\mathrm{e}^{-p}\right)\frac{1}{L}\int_{-L}^{0} U(z,t)\,\mathrm{d}z\right]^N,\end{aligned} \tag{15}$$

where we have assigned a general variable $z \equiv x_i$ as the motion of the particles is independent. Defining $P_{\mathrm{an}}(Q,t)$ as the probability distribution for Q in the annealed setting, we have

$$\sum_{Q=0}^{\infty} \mathrm{e}^{-pQ} P_{\mathrm{an}}(Q,t) = \overline{\langle \mathrm{e}^{-pQ}\rangle_{\{x_i\}}}. \tag{16}$$

Let us define the quantity $\mu_{\mathrm{an}}(L,t)$ as

$$\mu_{\mathrm{an}}(L,t) = \rho\int_{-L}^{0} U(z,t)\,\mathrm{d}z, \tag{17}$$

where the expression for $U(z,t)$ is given in equations (11) and (12) for the cases with one and two open boundaries respectively. For finite N, L, a small p expansion of equation (15) yields,

$$\begin{aligned}\overline{\langle \mathrm{e}^{-pQ}\rangle_{\{x_i\}}} &= \left[1-\left(1-\mathrm{e}^{-p}\right)\frac{1}{N}\mu_{\mathrm{an}}(L,t)\right]^N \\ &= 1-\mu_{\mathrm{an}}(L,t)\,p \\ &\quad + \left[\mu_{\mathrm{an}}(L,t) + \left(1-\frac{1}{N}\right)\mu_{\mathrm{an}}^2(L,t)\right]\frac{p^2}{2} + \mathcal{O}\left(p^3\right).\end{aligned} \tag{18}$$

Note that the terms associated with p and $p^2/2$ are the first and second moment of Q respectively (i.e. $\langle Q\rangle_{\mathrm{an}}$ and $\langle Q^2\rangle_{\mathrm{an}}$). From here, the mean and variance $\sigma_{\mathrm{an}}^2(L,t)$ of Q is found to be

$$\mu_{\mathrm{an}}(L,t) = \overline{\langle Q\rangle} = \langle Q\rangle_{\mathrm{an}}, \tag{19}$$

$$\begin{aligned}\sigma_{\mathrm{an}}^2(L,t) &= \overline{\langle Q^2\rangle} - \overline{\langle Q\rangle}^2 \\ &= \langle Q^2\rangle_{\mathrm{an}} - \langle Q\rangle_{\mathrm{an}}{}^2 \\ &= \mu_{\mathrm{an}}(L,t) - \frac{1}{\rho L}\mu_{\mathrm{an}}^2(L,t).\end{aligned} \tag{20}$$

In the above expression, we have replaced N by ρL. So far, the majority of studies on the dynamic behavior of Q have focused on infinite systems ($L \to \infty$). For an infinitely extended system with non-interacting particles, the mean and the variance are the same in the annealed setting. However, as we observe from equations (19) and (20), they are not identical when the system size is finite and furthermore, there is a L dependent correction term in the variance. In the limit $L\to\infty$ one recovers the known result, $\mu_{\text{an}}(L\to\infty,t)=\sigma^2_{\text{an}}(L\to\infty,t)$ [37].

3.2. Quenched setting

In the quenched setting, we first perform an average over the trajectories for a fixed initial condition and then average over the initial conditions of the system with a mean density ρ. Note the difference from the annealed case, where we average over the initial conditions and then compute the cumulant (see appendix C for more details). The generating function for Q in the quenched setting can be mathematically computed as

$$\sum_{Q=0}^{\infty} P_{\text{qu}}(Q,t)\,\mathrm{e}^{-pQ}=\exp\left[\overline{\ln\langle \mathrm{e}^{-pQ}\rangle_{\{x_i\}}}\right]. \tag{21}$$

Taking a logarithm of both sides of equation (13), we obtain

$$\ln\langle \mathrm{e}^{-pQ}\rangle_{\{x_i\}}=\sum_{i=1}^{N}\ln\left[1-\left(1-\mathrm{e}^{-p}\right)U(x_i,t)\right]. \tag{22}$$

Next performing an average over the initial positions in the above equation yield

$$\begin{aligned}\overline{\ln\langle \mathrm{e}^{-pQ}\rangle_{\{x_i\}}}&=\sum_{i=1}^{N}\frac{1}{L}\int_{-L}^{0}\ln\left[1-\left(1-\mathrm{e}^{-p}\right)U(x_i,t)\right]\mathrm{d}x_i\\&=\frac{N}{L}\int_{-L}^{0}\ln\left[1-\left(1-\mathrm{e}^{-p}\right)U(z,t)\right]\mathrm{d}z\\&=\rho\int_{-L}^{0}\ln\left[1-\left(1-\mathrm{e}^{-p}\right)U(z,t)\right]\mathrm{d}z\\&=I(p,t),\end{aligned} \tag{23}$$

where

$$I(p,t)=\rho\int_{-L}^{0}\ln\left[1-\left(1-\mathrm{e}^{-p}\right)U(z,t)\right]\mathrm{d}z. \tag{24}$$

Finally, we obtain the expression for the generating function for the distribution of Q in the quenched setting as

$$\sum_{Q=0}^{\infty} P_{\text{qu}}(Q,t)\,\mathrm{e}^{-pQ}=\exp\left[I(p,t)\right]. \tag{25}$$

Performing a small p expansion and collecting the terms at first and second orders of p (as also done for the annealed case), we obtain the expression for the mean $\mu_{\text{qu}}(L,t)$ and the variance $\sigma^2_{\text{qu}}(L,t)$ of Q in the quenched setting as

$$\mu_{\mathrm{qu}}(L,t) = \overline{\langle Q\rangle} = \langle Q\rangle_{\mathrm{qu}} = \mu_{\mathrm{an}}(L,t), \tag{26}$$

$$\begin{aligned}\sigma^2_{\mathrm{qu}}(L,t) &= \overline{\langle Q^2\rangle - \langle Q\rangle^2}\\ &= \langle Q^2\rangle_{\mathrm{qu}} - \langle Q\rangle_{\mathrm{qu}}{}^2\\ &= \mu_{\mathrm{qu}}(L,t) - \rho\int_{-L}^{0}\mathrm{d}z\, U^2(z,t),\end{aligned} \tag{27}$$

where $\mu_{\mathrm{qu}}(L,t) = \mu_{\mathrm{an}}(L,t)$ is given by equation (17). The mean in the annealed and quenched settings are the same even when the system size is finite. However, the higher-order cumulants are different.

In what follows, we study two specific examples of a system of diffusive particles and active RTPs.

4. Diffusive particles

In this section, we consider a set of diffusive particles initially confined in a finite one-dimensional box bounded between $[-L,0]$. We also consider two distinct set-ups; one in the presence of a reflecting boundary and the other with both boundaries open. We summarize the asymptotic behaviors of current fluctuations for both these cases in table 1.

We first focus on the case with a reflecting wall at $x = -L$.

4.1. One reflecting wall

In this section, we study the scenario where the boundary at $x = -L$ is a reflecting wall. The Green's function for a single diffusive Brownian particle in this case can be derived as [51]

$$G(x,t|x_i) = \frac{1}{\sqrt{4\pi Dt}}\left(\mathrm{e}^{-\frac{(2L+x+x_i)^2}{4Dt}} + \mathrm{e}^{-\frac{(x-x_i)^2}{4Dt}}\right), \tag{28}$$

which can be substituted in equation (11) to obtain

$$U(x_i,t) = \frac{1}{2}\left(1 + \mathrm{erf}\left(\frac{x_i}{2\sqrt{Dt}}\right) + \mathrm{erfc}\left(\frac{2L+x_i}{2\sqrt{Dt}}\right)\right), \tag{29}$$

where $\mathrm{erf}(z)$ and $\mathrm{erfc}(z)$ are the error function and complementary error function, respectively. Having obtained the expression for $U(x_i,t)$, we can now compute the expressions for the mean and the variance of Q for both annealed and quenched settings as detailed below.

4.1.1. Annealed setting.

Substituting equation (29) in equation (17), we obtain the expression for the mean of Q for a system of diffusing particles in the annealed setting as

$$\mu^{\mathrm{diff}}_{\mathrm{an}}(L,t) = \underbrace{\frac{\rho\sqrt{Dt}}{\sqrt{\pi}}}_{\text{infinite size limit}} \underbrace{+\rho L\left(\mathrm{erfc}\left(\frac{L}{\sqrt{Dt}}\right) - \frac{\sqrt{Dt}}{\sqrt{\pi}L}\mathrm{e}^{-\frac{L^2}{Dt}}\right)}_{\text{finite size correction}}. \tag{30}$$

The first term in the mean does not have any explicit dependence on the system size L. This is the result one expects in the case of an infinite system size limit ($L\to\infty$). The second term

Table 1. Asymptotic behavior of current fluctuations for diffusive motion in the annealed and quenched settings.

	$t \to 0$	$t \to \infty$	
Diffusion reflecting boundary	$\frac{\rho\sqrt{Dt}}{\sqrt{\pi}}$	$\frac{\rho L^2}{\sqrt{\pi}\sqrt{Dt}}$	$\sigma_{\text{an}}^{\text{diff}}(L,t)^2$
	$\frac{1}{\sqrt{2}}\frac{\rho\sqrt{Dt}}{\sqrt{\pi}}$	$\frac{\rho L^2}{\sqrt{\pi}\sqrt{Dt}}$	$\sigma_{\text{qu}}^{\text{diff}}(L,t)^2$
Diffusion finite interval	$2\frac{\rho\sqrt{Dt}}{\sqrt{\pi}}$	$\frac{1}{2}\frac{\rho L^2}{\sqrt{\pi}\sqrt{Dt}}$	$\sigma_{\text{an}}^{\text{diff}}(L,t)^2$
	$\sqrt{2}\frac{\rho\sqrt{Dt}}{\sqrt{\pi}}$	$\frac{1}{2}\frac{\rho L^2}{\sqrt{\pi}\sqrt{Dt}}$	$\sigma_{\text{qu}}^{\text{diff}}(L,t)^2$

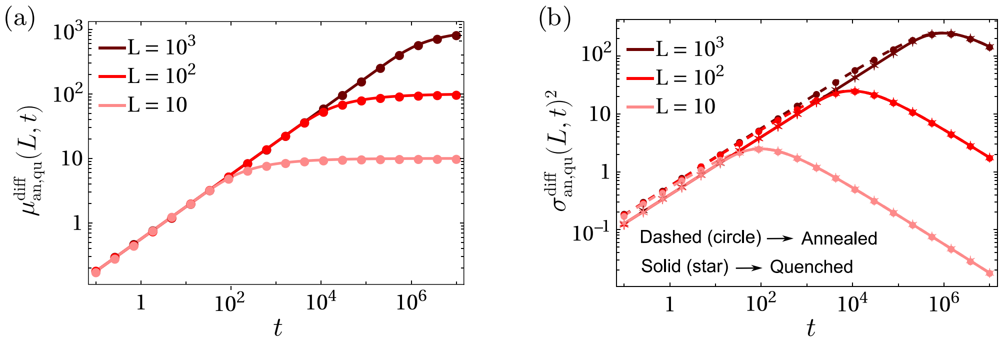

Figure 3. Behavior of the (a) mean and the (b) variance of current through the origin in the presence of a reflecting wall at $x = -L$ for N diffusive Brownian particles. The mean in the annealed and quenched settings are the same. The variance in the quenched setting (solid curves) differs from the annealed (dashed curves) by a factor of $\sqrt{2}$ at times $t \ll L^2/D$, however, they become equal at times $t \gg L^2/D$. The parameter values used are $\rho = 1, D = 1$. Note that $\rho = 1$ automatically implies $N = L$. The stars and circles represent the results obtained through numerical simulations of the microscopic model for the quenched and annealed settings respectively.

in the parentheses contains the finite size corrections which vanishes in the limit $L \to \infty$. The expression for the variance follows from equation (20) as

$$\sigma_{\text{an}}^{\text{diff}}(L,t)^2 = \mu_{\text{an}}^{\text{diff}}(L,t) - \frac{1}{\rho L}\mu_{\text{an}}^{\text{diff}}(L,t)^2, \tag{31}$$

with $\mu_{\text{an}}^{\text{diff}}(L,t)$ given by equation (30). Since the exact expression for the variance is quite lengthy, we do not provide it here. Figure 3 shows the behavior of the mean and the variance as a function of time obtained from equations (30) and (31) for different system sizes keeping the density $\rho = 1$ fixed. The result matches well with that obtained from numerical simulation (see appendix C for a detailed discussion on the simulation procedure).

Both the mean and variance increase monotonically with time for $t \ll L^2/D$. Taking this limit in equations (30) and (31), we obtain

$$\mu_{\text{an}}^{\text{diff}}\left(L, t \ll L^2/D\right) \approx \frac{\rho\sqrt{Dt}}{\sqrt{\pi}}, \tag{32}$$

$$\sigma_{\text{an}}^{\text{diff}}\left(L, t \ll L^2/D\right)^2 \approx \frac{\rho\sqrt{Dt}}{\sqrt{\pi}}. \tag{33}$$

At very short time scales, the mean and the variance in the annealed setting are the same and also correspond to the infinite system results. However, at larger time scales $t \gg L^2/D$, the mean saturates to the value N and the variance goes to zero as

$$\mu_{\text{an}}^{\text{diff}}\left(L, t \gg L^2/D\right) \approx N - \frac{\rho L^2}{\sqrt{\pi}\sqrt{Dt}}, \tag{34}$$

$$\sigma_{\text{an}}^{\text{diff}}\left(L, t \gg L^2/D\right)^2 \approx \frac{\rho L^2}{\sqrt{\pi}\sqrt{Dt}}. \tag{35}$$

In deriving the asymptotic time limits we have used the following properties of the complementary error function

$$\text{erfc}(z) \approx \begin{cases} 1 - \frac{2z}{\sqrt{\pi}}, & \text{when } z \to 0, \\ \frac{e^{-z^2}}{\sqrt{\pi}z}, & \text{when } z \to \infty. \end{cases} \tag{36}$$

At very short times, particles that are close to the boundary at $x = 0$ can only get out of the region $[-L, 0]$. Meanwhile, particles that are situated near the boundary at $x = -L$ do not get sufficient time to escape through the origin. In effect, the finite size of the system does not come into the picture at very short times. Consequently, the results obtained match with those obtained for the case of an infinite system. (Here we emphasize that generally, it is not true that all the particles near the origin are expected to get out at short times. As shown in [52] some particles may start going in a completely opposite direction to the origin as well. However, we are considering only those particles which are coming out of the origin.) Conversely, as time progresses, particles in the bulk or near the reflecting wall at $x = -L$ have sufficient time to exit the box through the origin. It is expected that eventually, all N particles will exit this region, resulting in a mean current of N. At these large time scales, with all particles leaving the box, the variance tends to approach zero.

4.1.2. Quenched setting. From equation (26) we see that the mean in the quenched setting is the same as the annealed setting. Therefore we obtain

$$\mu_{\text{qu}}^{\text{diff}}(L, t) = \mu_{\text{an}}^{\text{diff}}(L, t), \tag{37}$$

with the limiting behaviors given in equations (32) and (34).

Calculating the variance in the quenched setting is challenging because the integral in equation (27) cannot be explicitly computed. However, we can determine the asymptotic behaviors of the variance of Q using simple arguments. At short times ($t \ll L^2/D$), the system does not experience the effects of finite size and the results obtained are similar to those obtained for infinite systems (as also seen for the annealed case). We thus take the limit $L \to \infty$ in equation (29) to obtain

$$U(x_i, t) \xrightarrow[L \to \infty]{} \frac{1}{2}\left(1 + \text{erf}\left(\frac{x_i}{2\sqrt{Dt}}\right)\right). \tag{38}$$

Using this result, the integration in equation (27) can be easily performed to obtain

$$\sigma_{\text{qu}}^{\text{diff}}\left(L, t \ll L^2/D\right)^2 \approx \frac{\rho\sqrt{Dt}}{\sqrt{2\pi}}. \tag{39}$$

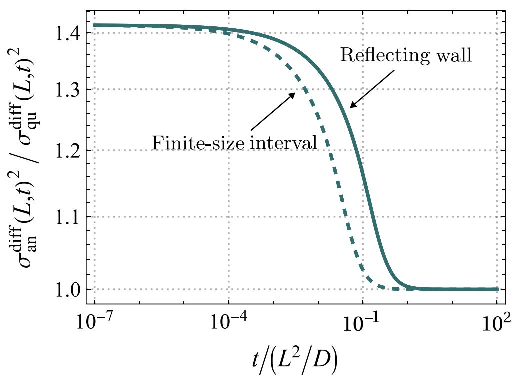

Figure 4. The ratio of the variance of Q in the annealed and quenched settings plotted against rescaled time $t/(L^2/D)$ for two different set-ups: (a) in the presence of a reflecting wall (the solid line) and (b) when both sides are open (the dashed line). The variance in the annealed setting is given by equation (20) and the variance in the quenched setting has been numerically evaluated using equation (27), for $L = 10, 10^2, 10^3$ and $D = 1$. Note that here curves for different values of L collapse to a single master curve shown by the green color. When $t \ll L^2/D$, the ratio is $\sqrt{2}$, and when $t \gg L^2/D$, the variances in the annealed and quenched settings become exactly equal and the ratio becomes unity.

Similarly, at very large times $t \gg L^2/D$, one can take the limit $L \to 0$ to obtain

$$U(x_i,t) \xrightarrow[L\to 0]{} 1 - \frac{L e^{-\frac{x_i^2}{4Dt}}}{\sqrt{\pi}\sqrt{Dt}}. \tag{40}$$

We next compute the integral in equation (27) in this limit yielding

$$\sigma_{\mathrm{qu}}^{\mathrm{diff}}\left(L, t \gg L^2/D\right)^2 \approx \frac{\rho L^2}{\sqrt{\pi}\sqrt{Dt}}. \tag{41}$$

Note that, at time scales where finite size effects are not present ($t \ll L^2/D$), the variance for the quenched setting given in equation (39) is suppressed by a factor of $\sqrt{2}$ compared to the annealed setting provided in equation (33). However at time scales $t \gg L^2/D$, the finite size effects are dominant and the variance in the quenched and annealed settings become exactly equal to each other. Figure 3 shows the behavior of the mean and the variance as a function of time for both annealed and quenched settings. The mean is given by equation (30) for both annealed and quenched settings. The variance is given by equation (20) in the annealed setting and by equation (27) in the quenched setting. The variance in the quenched case at all times is obtained through numerical integration of equation (27) using Mathematica. Figure 4 displays the plot of the ratio of the variance in the annealed and quenched settings as a function of the rescaled time $t/(L^2/D)$ for different system sizes $L = 10, 10^2$ and 10^3. All the curves for different system sizes collapse into a single curve. This in turn implies that the ratio of the variances in the annealed and quenched scenarios is independent of re-scaled time $t/(L^2/D)$. At time scales $t \ll L^2/D$, finite size effects can be neglected and the ratio is close to $\sqrt{2}$. However at large time scales $t \gg L^2/D$, the finite size effects become prominent. Consequently, the annealed and the quenched averages become the same, and the ratio becomes one. Intuitively, the convergence of variances in the annealed and quenched settings at large times can be attributed to the fact that the system remembers the initial condition only up to a timescale $\sim L^2/D$.

This in turn implies that the effects of the initial averaging procedure should be negligible beyond this time scale.

4.2. Finite size interval

We next focus on the case where there is no reflecting wall in the system so that particles can escape through either of the boundaries at $x = 0$ or $x = -L$. The diffusion propagator in this case is given by

$$G(x,t|x_i) = \frac{1}{\sqrt{4\pi Dt}} \mathrm{e}^{-\frac{(x-x_i)^2}{4Dt}}. \tag{42}$$

Substituting this expression in equation (12), we obtain

$$U(x_i,t) = \frac{1}{2}\left(1 + \operatorname{erf}\left(\frac{x_i}{2\sqrt{Dt}}\right) + \operatorname{erfc}\left(\frac{L+x_i}{2\sqrt{Dt}}\right)\right). \tag{43}$$

We next focus on annealed and quenched settings separately.

4.2.1. Annealed setting. We substitute equation (43) in the expression for mean provided in equation (17). This yields the exact expression for the mean in the annealed setting as

$$\mu_{\mathrm{an}}^{\mathrm{diff}}(L,t) = \underbrace{\frac{2\rho\sqrt{Dt}}{\sqrt{\pi}}}_{\text{infinite size limit}} \underbrace{+\rho L\left(\operatorname{erfc}\left(\frac{L}{2\sqrt{Dt}}\right) - \frac{2\sqrt{Dt}}{\sqrt{\pi}L}\mathrm{e}^{-\frac{L^2}{4Dt}}\right)}_{\text{finite size correction}}. \tag{44}$$

In the asymptotic limit, we obtain the simplified expressions

$$\mu_{\mathrm{an}}^{\mathrm{diff}}(L,t) \approx \begin{cases} \frac{2\rho\sqrt{Dt}}{\sqrt{\pi}}, & t \ll L^2/D, \\ N - \frac{\rho L^2}{2\sqrt{\pi}\sqrt{Dt}}, & t \gg L^2/D. \end{cases} \tag{45}$$

The expression for the variance of Q can now be exactly computed using equations (31) and (44). Since this expression is quite long, we do not quote it here. Figure 5 shows the behavior of the mean and the variance as a function of time obtained from equations (31) and (44) for different system sizes keeping the density $\rho = 1$ fixed. In the asymptotic limits, we obtain the simple expressions,

$$\sigma_{\mathrm{an}}^{\mathrm{diff}}(L,t)^2 \approx \begin{cases} \frac{2\rho\sqrt{Dt}}{\sqrt{\pi}}, & t \ll L^2/D, \\ \frac{\rho L^2}{2\sqrt{\pi}\sqrt{Dt}}, & t \gg L^2/D. \end{cases} \tag{46}$$

At short times, the variance is larger by a factor of 2 as compared to the case with a single reflecting boundary in the annealed setting. However, at large times, the variance is lesser by a factor of 2 as compared to the previous case.

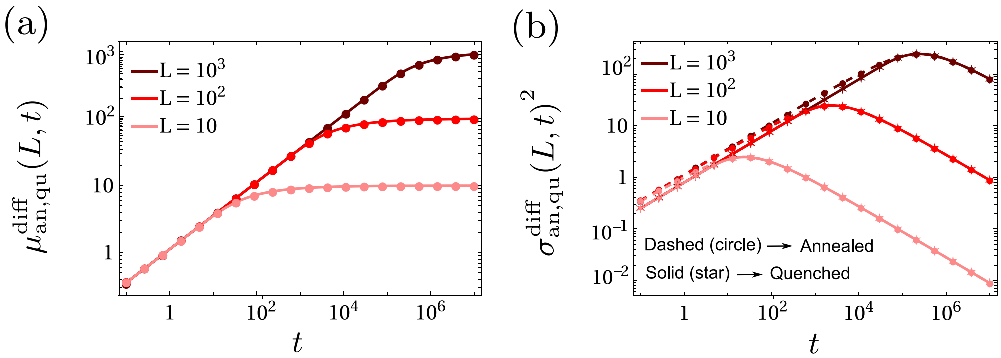

Figure 5. Behavior of the (a) mean and the (b) variance of Q as a function of time when both the boundaries at $x = 0, -L$ are open for a diffusive system. The mean in the annealed and quenched settings are the same. The variance in the quenched setting (solid curves) differs from the annealed (dashed curves) by a factor of $\sqrt{2}$ at times $t \ll L^2/D$, however, they become equal at times $t \gg L^2/D$. The parameter values used are $\rho = 1, D = 1$. The stars and circles represent the results obtained through numerical simulations of the microscopic model for the quenched and annealed settings respectively.

4.2.2. Quenched setting. The expression for the mean in the quenched setting is the same as the annealed setting and is given in equation (44). It is difficult to compute the exact closed-form expression for the variance in the quenched setting using the expression for $U(x_i, t)$ provided in equation (43). Nevertheless, it is possible to perform a careful asymptotic analysis in the Laplace space (details are given in appendix A) which yields

$$\sigma_{\mathrm{qu}}^{\mathrm{diff}}(L,t)^2 \approx \begin{cases} \frac{\sqrt{2}\rho\sqrt{Dt}}{\sqrt{\pi}}, & t \ll \frac{L^2}{D}, \\ \frac{\rho L^2}{2\sqrt{\pi}\sqrt{Dt}}, & t \gg \frac{L^2}{D}. \end{cases} \tag{47}$$

Similar to the case with a reflecting wall, the variance in the annealed and quenched settings are distinct at short times ($t \ll L^2/D$) and become exactly equal to each other at times $t \gg L^2/D$. Figure 5 shows the behavior of the mean and the variance as a function of time for both annealed and quenched settings. The mean is given by equation (44) for both annealed and quenched settings. The variance is given by equation (20) in the annealed setting and by equation (27) in the quenched setting. As mentioned earlier the variance in the quenched scenario is obtained by numerical integration of equation (27). In figure 4 we display a plot of the exact ratio of the variance in the annealed to the quenched setting. Again we find that all the curves merge to a single master curve as shown by the dashed one when the time is re-scaled to $t/(L^2/D)$. As before, even in the quenched setting, the variance of Q is larger by a factor of 2 compared to the case with a single reflecting boundary at short times. However, at large times, the variance is lower by a factor of 2. This demonstrates how boundary conditions can influence the transport properties of stochastic systems over time.

5. Run-and-Tumble particles (RTPs)

In this section, we analyze the statistics of the integrated current Q in a one-dimensional system of non-interacting RTPs. The dynamics of an RTP consist of run and tumble phases. During

Table 2. Asymptotic behavior of current fluctuations for run and tumble particle motion in the annealed and quenched settings.

	$t \to 0$	$t \to \infty$	
RTP reflecting boundary	$\frac{1}{2}\rho v t$	$\frac{\rho L^2}{\sqrt{\pi}\sqrt{D_{\text{eff}} t}}$	$\sigma_{\text{an}}^{\text{rtp}}(L,t)^2$
	$\frac{1}{4}\rho v t$	$\frac{\rho L^2}{\sqrt{\pi}\sqrt{D_{\text{eff}} t}}$	$\sigma_{\text{qu}}^{\text{rtp}}(L,t)^2$
RTP finite interval	$\rho v t$	$\frac{1}{2}\frac{\rho L^2}{\sqrt{\pi}\sqrt{D_{\text{eff}} t}}$	$\sigma_{\text{an}}^{\text{rtp}}(L,t)^2$
	$\frac{1}{2}\rho v t$	$\frac{1}{2}\frac{\rho L^2}{\sqrt{\pi}\sqrt{D_{\text{eff}} t}}$	$\sigma_{\text{qu}}^{\text{rtp}}(L,t)^2$

the run phase, the particle moves with a constant velocity v and during the tumble phase, the particle instantaneously changes its direction of velocity. The Langevin equation governing the motion of an RTP can be written as

$$\frac{\mathrm{d}x}{\mathrm{d}t} = v\sigma(t), \tag{48}$$

where $\sigma(t) = \pm 1$ is a dichotomous noise and it switches between the two values after a random time τ which is distributed according to an exponential distribution $p(\tau) = \gamma \mathrm{e}^{-\gamma\tau}$. The asymptotic behaviors of current fluctuations for non-interacting RTPs in various settings are summarized in table 2.

As for the diffusive case, we first focus on the situation with a reflecting wall at $x = -L$.

5.1. One reflecting wall

The boundary conditions for an RTP in the presence of a reflecting wall have to be defined carefully. After a reflection from the wall, each particle has two possibilities for its orientation, (i) it continues to move in the same direction i.e. towards the wall or (ii) it changes the orientation after reflection and starts moving away from the wall. In this paper, we consider the latter case where velocity is reversed after each reflection. This prevents the accumulation of particles near the wall [53]. The Green's function for RTP has a simple form in the Laplace space. The Laplace transform of a function $f(t)$ is defined as $\widetilde{f}(s) = \int_0^t \mathrm{d}t f(t)\mathrm{e}^{-st}$. The propagator of RTP can be computed using the image method as [51]

$$\widetilde{G}(x,s|x_i) = \frac{\sqrt{s(s+2\gamma)}}{2vs}\left(\mathrm{e}^{-\frac{\sqrt{s(s+2\gamma)}}{v}|x-x_i|} + \mathrm{e}^{-\frac{\sqrt{s(s+2\gamma)}}{v}|x+2L+x_i|}\right). \tag{49}$$

Using equation (11), we next compute the Laplace transform of $U(x_i,t)$ as,

$$\widetilde{U}(x_i,s) = \frac{\mathrm{e}^{\frac{x_i\sqrt{s(2\gamma+s)}}{v}}}{2s} + \frac{\mathrm{e}^{-\frac{(2L+x_i)\sqrt{s(2\gamma+s)}}{v}}}{2s}. \tag{50}$$

In the subsequent sections, we focus on the annealed and quenched settings separately.

5.1.1. Annealed setting.

We take a Laplace transform of the expression for the mean provided in equation (17) to obtain

$$\widetilde{\mu}_{\text{an}}(L,s) = \rho\int_{-L}^{0}\widetilde{U}(z,s)\,\mathrm{d}z. \tag{51}$$

Substituting equation (50) in the above equation, we obtain the expression for the mean of Q in Laplace space as

$$\widetilde{\mu}_{\text{an}}^{\text{rtp}}(L,s) = \underbrace{\frac{\rho v}{2s\sqrt{s(2\gamma+s)}}}_{\text{infinite size limit}} - \underbrace{\frac{\rho v \mathrm{e}^{-\frac{2L\sqrt{s(2\gamma+s)}}{v}}}{2s\sqrt{s(2\gamma+s)}}}_{\text{finite size correction}}. \tag{52}$$

The first term in the above expression represents the infinite size ($L \to \infty$) limit while the second term is a finite size correction. Since the exact inversion of the above expression is difficult, we focus on the asymptotic behaviors taking different limits of s as explained below.

For RTPs, there are two important time scales, (i) one timescale is associated with the mean run time $t = 1/\gamma$ between consecutive tumbles and (ii) the other timescale is associated with the finite size of the system $t = L^2/D_{\text{eff}}$ where $D_{\text{eff}} = v^2/2\gamma$ is the effective diffusion constant for an RTP in one dimension. At very large times, $t \gg 1/\gamma$ the statistical properties of an RTP become similar to that of a Brownian particle with an effective diffusion constant D_{eff}. In this paper, we consider the case where $L^2/D_{\text{eff}} \gg 1/\gamma$. Thus the limit $s \to \infty$ corresponds to timescales $t \ll L^2/D_{\text{eff}}$. In this limit, we observe that the second term in equation (52) is exponentially suppressed as compared to the first term and we obtain

$$\widetilde{\mu}_{\text{an}}^{\text{rtp}}(L,s) \xrightarrow[s\to\infty]{} \frac{\rho v}{2s\sqrt{s(2\gamma+s)}}, \tag{53}$$

which upon inversion yields

$$\mu_{\text{an}}^{\text{rtp}}\left(L, t \ll L^2/D_{\text{eff}}\right) = \frac{\rho v t}{2}\mathrm{e}^{-\gamma t}\left(I_0(t\gamma) + I_1(t\gamma)\right), \tag{54}$$

where $I_0(z)$ and $I_1(z)$ are the modified Bessel functions of the first kind. The asymptotic behaviors of the modified Bessel function of the first kind (and order ν) are given as

$$I_\nu(z) \approx \begin{cases} z^\nu\left(\frac{2^{-\nu}}{\Gamma(\nu+1)} + \frac{2^{-\nu-2}z^2}{(\nu+1)\Gamma(\nu+1)}\right), & \text{when } z \to 0, \\ \frac{\mathrm{e}^z}{\sqrt{2\pi}\sqrt{z}}, & \text{when } z \to \infty. \end{cases} \tag{55}$$

Substituting these expressions in equation (54), one obtains the limiting behaviors of the mean of Q as

$$\mu_{\text{an}}^{\text{rtp}}(L,t) \approx \begin{cases} \frac{1}{2}\rho v t, & t \ll 1/\gamma, \\ \frac{\rho\sqrt{D_{\text{eff}}t}}{\sqrt{\pi}}, & \frac{1}{\gamma} \ll t \ll \frac{L^2}{D_{\text{eff}}}. \end{cases} \tag{56}$$

To obtain the large time ($t \gg L^2/D_{\text{eff}}$) behavior, we take the $s \to 0$ limit of the expression provided in equation (52) yielding

$$\widetilde{\mu}_{\text{an}}^{\text{rtp}}(L,s) \xrightarrow[s\to 0]{} \frac{N}{s} - \frac{\rho L^2}{\sqrt{D_{\text{eff}}}\sqrt{s}}, \tag{57}$$

which upon inversion yields

$$\mu_{\text{an}}^{\text{rtp}}\left(L, t \gg L^2/D_{\text{eff}}\right) = N - \frac{\rho L^2}{\sqrt{\pi}\sqrt{D_{\text{eff}}t}}. \tag{58}$$

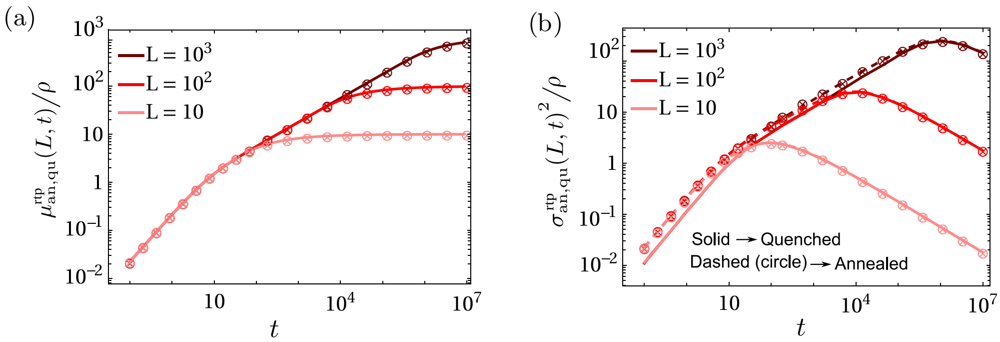

Figure 6. Behavior of the (a) mean and the (b) variance in both annealed and quenched settings for RTP in the presence of a reflecting wall at $x = -L$. The mean in the annealed and quenched settings are the same. The variance in the quenched setting (solid curves) differs from the annealed (dashed curves) by a factor of 2 at times $t \ll L^2/D_{\mathrm{eff}}$, however, they become equal at times $t \gg L^2/D_{\mathrm{eff}}$. The parameter values used are $v = \sqrt{0.2}, \gamma = 0.1$ to have $D_{\mathrm{eff}} = v^2/2\gamma = 1$. Values of ρ is chosen distinctly for each value of L (details in appendix C). The circles with crosses represent the results obtained through numerical simulations of the microscopic model and the dashed curves represent the results obtained through numerical Laplace inversion of equation (52) along with equation (20) for the annealed setting. The variance in quenched setting (solid curves) has been obtained through microscopic simulations.

The asymptotic behavior of the variance can be found by substituting the asymptotic expressions for the mean provided in equations (54) and (58) directly in equation (20). This yields

$$\sigma^{\mathrm{rtp}}_{\mathrm{an}}(L,t)^2 \approx \begin{cases} \frac{1}{2}\rho v t, & t \ll 1/\gamma, \\ \frac{\rho\sqrt{D_{\mathrm{eff}} t}}{\sqrt{\pi}}, & \frac{1}{\gamma} \ll t \ll \frac{L^2}{D_{\mathrm{eff}}}, \\ \frac{\rho L^2}{\sqrt{\pi}\sqrt{D_{\mathrm{eff}} t}} & t \gg L^2/D_{\mathrm{eff}}. \end{cases} \tag{59}$$

At time scales $t \gg 1/\gamma$, the mean and the variance behave similar to that of the diffusive case as in equations (32)–(35) with the diffusion constant D replaced by D_{eff}. Figure 6 shows the behavior of the mean and the variance as a function of time obtained through numerical Laplace inversion (via inbuilt resource function in Mathematica) of equation (52) and using these results in equation (20).

5.1.2. Quenched setting. Similar to the case of diffusion, the mean in the quenched setting is the same as that in the annealed setting. That is,

$$\mu^{\mathrm{rtp}}_{\mathrm{qu}}(L,t) = \mu^{\mathrm{rtp}}_{\mathrm{an}}(L,t). \tag{60}$$

The exact asymptotic behaviors of the mean are provided in equations (54) and (58). The asymptotic limits for the variance can be computed using similar arguments we applied for the diffusive case. At very short times $t \ll L^2/D_{\mathrm{eff}}$, we take the limit $L \to \infty$ in equation (50) and follow a similar calculation as we did for the diffusive case to obtain

$$\begin{aligned}\sigma^{\mathrm{rtp}}_{\mathrm{qu}}(L, t \ll L^2/D_{\mathrm{eff}})^2 = \frac{\rho v}{8} t e^{-2\gamma t}\left[(4+\pi L_0(2\gamma t)) I_1(2\gamma t)\right. \\ \left. +(2-\pi L_1(2\gamma t)) I_0(2\gamma t)\right],\end{aligned} \tag{61}$$

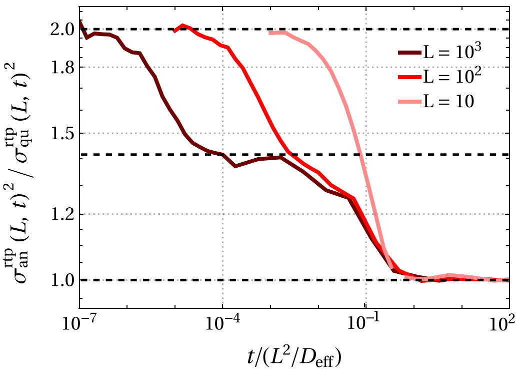

Figure 7. Ratio of the variances of Q in the annealed and quenched settings for RTPs in the presence of a reflecting wall. For small timescales ($t \ll 1/\gamma$), the ratio is 2. With time it starts decreasing and at intermediate time scales $1/\gamma \ll t \ll L^2/D_{\rm eff}$, the ratio saturates to the value $\sqrt{2}$. This saturation is more evident for system size $L = 10^3$ as the intermediate region is broad here. At time scale $t \gg L^2/D_{\rm eff}$ all the curves merge and eventually saturate to unity. While computing the ratio, the numerator has been obtained through numerical Laplace inversion of equation (52) along with equation (20) while the denominator has been estimated using microscopic simulations.

where $L_0(z), L_1(z)$ are the modified Struve functions. Further depending on the time scale $1/\gamma$, we obtain the limiting behaviors for the variance of Q

$$\sigma_{\rm qu}^{\rm rtp}(L,t)^2 \approx \begin{cases} \frac{1}{4}\rho v t, & t \ll 1/\gamma, \\ \frac{\rho\sqrt{D_{\rm eff}t}}{\sqrt{2\pi}}, & \frac{1}{\gamma} \ll t \ll \frac{L^2}{D_{\rm eff}}. \end{cases} \tag{62}$$

Here, we have used the following asymptotic behaviors of the Struve functions

$$L_\nu(z) \approx \begin{cases} z^\nu\left(\frac{2^{-\nu}z}{\sqrt{\pi}\,\Gamma\left(\nu+\frac{3}{2}\right)} + \frac{2^{-\nu-1}z^3}{3\sqrt{\pi}\,\Gamma\left(\nu+\frac{5}{2}\right)}\right), & \text{when } z \to 0, \\ \frac{e^z}{\sqrt{2\pi}\sqrt{z}}, & \text{when } z \to \infty. \end{cases} \tag{63}$$

The large-time asymptotic behavior of the variance can be computed by taking the limit $L \to \infty$ in equation (50) and performing a similar calculation as for the diffusive case, or it can be derived directly from the fact that at this timescale, the statistical properties of an RTP is similar to that of a Brownian particle with a modified diffusion constant $D = D_{\rm eff}$. We thus obtain from equation (27)

$$\sigma_{\rm qu}^{\rm rtp}\left(t \gg L^2/D_{\rm eff}\right)^2 = \frac{\rho L^2}{\sqrt{\pi}\sqrt{D_{\rm eff}t}}, \tag{64}$$

which is the same as the large time behavior of the variance in the annealed setting given in equation (59). Figure 6 displays the behavior of the mean and the variance as a function of time for both annealed and quenched settings. The mean is given by numerical inversion of equation (52) for both annealed and quenched settings. The variance in the quenched case was obtained only with numerical simulation as described in appendix C. Figure 7 displays the plot of the ratio of the variance in the annealed and quenched settings as a function of the rescaled time $t/(L^2/D_{\rm eff})$ for different system sizes $L = 10, 10^2$ and 10^3. Unlike the diffusive case, the curves do not collapse into a single curve as RTPs have different timescales involved in addition to the diffusion timescale. At time scales $t \ll 1/\gamma$, finite size effects can be neglected and the ratio is close to 2. We see that at intermediate time scales $1/\gamma \ll t \ll L^2/D_{\text{eff}}$, the ratio saturates close to the value $\sqrt{2}$. However at large time scales $t \gg L^2/D_{\text{eff}}$, the finite size effects become prominent. Consequently, the annealed and the quenched averages become the same, and the ratio becomes one.

5.2. *Finite size interval*

We next focus on the case where the particles can escape either through the boundary at $x = 0$ or $x = -L$. The propagator for an RTP in the Laplace space is given as [37]

$$\widetilde{G}(x, s|x_i) = \frac{\sqrt{s(s+2\gamma)}}{2vs} \mathrm{e}^{-\frac{\sqrt{s(s+2\gamma)}}{v}|x-x_i|}. \tag{65}$$

Substituting this expression in equation (12), we obtain

$$\widetilde{U}(x_i, s) = \frac{\mathrm{e}^{\frac{x_i\sqrt{s(2\gamma+s)}}{v}}}{s} + \frac{\mathrm{e}^{\frac{-(L+x_i)\sqrt{s(2\gamma+s)}}{v}}}{s}. \tag{66}$$

We next focus on the cases of annealed and quenched averages separately.

5.2.1. *Annealed setting.*

We first focus on the annealed setting where the positions of the particles are allowed to fluctuate initially. Substituting equation (66) in equation (51) we obtain the expression for the mean in Laplace space as

$$\widetilde{\mu}_{\text{an}}^{\text{rtp}}(L, s) = \underbrace{\frac{\rho v}{s\sqrt{s(2\gamma+s)}}}_{\text{infinite size limit}} - \underbrace{\frac{\rho v \mathrm{e}^{-\frac{L\sqrt{s(2\gamma+s)}}{v}}}{s\sqrt{s(2\gamma+s)}}}_{\text{finite size correction}}. \tag{67}$$

Using this expression, the asymptotic behaviors of the mean and the variance in real-time can be computed as before. For the mean, we obtain

$$\mu_{\text{an}}^{\text{rtp}}(L, t) \approx \begin{cases} \rho v t, & t \ll 1/\gamma, \\ \frac{2\rho\sqrt{D_{\text{eff}} t}}{\sqrt{\pi}}, & \frac{1}{\gamma} \ll t \ll \frac{L^2}{D_{\text{eff}}}, \\ N - \frac{\rho L^2}{2\sqrt{\pi}\sqrt{D_{\text{eff}} t}} & t \gg L^2/D_{\text{eff}}. \end{cases} \tag{68}$$

and for the variance, we obtain

$$\sigma_{\text{an}}^{\text{rtp}}(L, t)^2 \approx \begin{cases} \rho v t, & t \ll 1/\gamma, \\ \frac{2\rho\sqrt{D_{\text{eff}} t}}{\sqrt{\pi}}, & \frac{1}{\gamma} \ll t \ll \frac{L^2}{D_{\text{eff}}}, \\ \frac{\rho L^2}{2\sqrt{\pi}\sqrt{D_{\text{eff}} t}} & t \gg L^2/D_{\text{eff}}. \end{cases} \tag{69}$$

The behavior of the mean and the variance in the annealed setting is shown in figure 8. The mean at all times is obtained through numerical Laplace inversion of equation (67) via Mathematica and the variance was obtained by plugging the mean in equation (20).

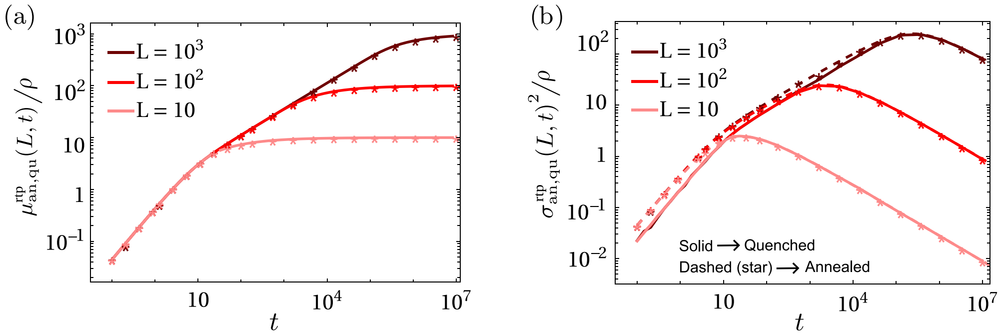

Figure 8. Behavior of the (a) mean and the (b) variance in both annealed and quenched settings for run-and-tumble particles when both sides at $x = 0, -L$ are open. The mean in the annealed and quenched settings are the same. The variance in the quenched setting (solid curves) differs from the annealed (dashed curves) by a factor of 2 at times $t \ll L^2/D_{\text{eff}}$, however, they become equal at times $t \gg L^2/D_{\text{eff}}$. The parameter values used are $v = \sqrt{0.2}, \gamma = 0.1$ so that $D_{\text{eff}} = v^2/2\gamma = 1$. Values of ρ is chosen distinctly for each value of L (details in appendix C). The stars represent the results obtained through numerical simulations of the microscopic model and the dashed curves represent the results obtained through numerical Laplace inversion of equation (67) along with equation (20) for the annealed setting. The variance in quenched setting (solid curves) has been entirely obtained through microscopic simulations.

5.2.2. Quenched setting. The mean in the quenched setting is the same as the mean in the annealed setting and is given in equation (67). Since it is difficult to find the exact expression of the variance in the quenched setting in closed form, we focus on the asymptotic behaviors. A careful asymptotic analysis in the Laplace space (details given in appendix B) yields

$$\sigma_{\text{qu}}^{\text{rtp}}(L,t)^2 \approx \begin{cases} \frac{1}{2}\rho v t, & t \ll \frac{1}{\gamma}, \\ \frac{\rho L^2}{2\sqrt{\pi D_{\text{eff}} t}}, & t \gg \frac{L^2}{D_{\text{eff}}}. \end{cases} \tag{70}$$

Figure 8 displays the behavior of the mean and the variance as a function of time for both annealed and quenched settings. The mean is given by numerical inversion of equation (67) for both annealed and quenched settings. We found the variance in the quenched case at all times only through numerical simulations. In figure 9, we display a plot of the ratio of the variance in the annealed and quenched settings as a function of the rescaled time $t/(L^2/D_{\text{eff}})$ for different system sizes $L = 10, 10^2$ and 10^3. Similar to the set-up with a reflecting wall, the curves do not collapse into a single curve as RTPs have different timescales involved in addition to the diffusion timescale. At time scales $t \ll 1/\gamma$, the ratio is close to 2. At intermediate time scales $1/\gamma \ll t \ll L^2/D_{\text{eff}}$, the ratio is close to the value $\sqrt{2}$. However at large time scales $t \gg L^2/D_{\text{eff}}$, the finite size effects become prominent and the ratio saturates to 1. Compared to the reflecting case, the variance is larger by a factor of 2 at times $t \ll L^2/D_{\text{eff}}$. However, at large times, the variance gets suppressed by a factor of 2 as compared to the reflecting case. This is exactly the same behavior we observed for the system of diffusing particles. This demonstrates how boundary conditions can influence the transport properties of stochastic systems over time. A more intricate understanding of these various factors would require a detailed study of current fluctuations in different system geometries across various spatial dimensions.

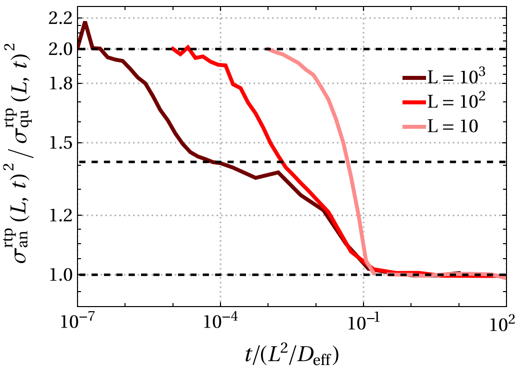

Figure 9. Ratio of the variance of Q in the annealed and quenched settings for RTPs in a finite-sized interval with open boundaries. The variance in the annealed setting has been obtained through numerical Laplace inversion of equation (67) along with equation (20). The variance in the quenched setting has been obtained through numerical simulations of the microscopic model. Unlike the Brownian case, the curves for different system sizes L do not collapse into a single curve at short and intermediate times. However, when $t \gg L^2/D_{\mathrm{eff}}$, all the curves merge and saturate to the value 1.

6. Discussion and outlook

In this paper, we have studied the fluctuations in the number of particles exiting the boundaries of a finite-sized one-dimensional box $x \in [-L, 0]$. We investigated specific examples of passive as well as active systems; namely non-interacting diffusive and RTPs respectively. We started from a uniform distribution of particles inside the box and obtained the statistical properties of the integrated current for two distinct setups: (i) where both the boundaries at $x = -L, 0$ are open so that particles can cross through either of them and (ii) when the boundary at $x = -L$ is reflecting in nature so that particles can only pass through the boundary at $x = 0$. We found that the properties of the current depend on how the initial conditions are averaged out. We also demonstrated two distinct procedures of such averages in this paper; annealed and quenched averages. We showed how the results from both these averages depend on the finite size of the box L.

For the system of diffusive particles, we showed that the ratio of fluctuations in the annealed and quenched settings changes from a value of $\sqrt{2}$ at short times ($t \ll L^2/D$) to 1 at large times ($t \gg L^2/D$). While for RTPs, this ratio changes from a value of 2 at short times ($t \ll 1/\gamma$) to 1 at large times ($t \gg L^2/D_{\mathrm{eff}}$) through an intermediate saturation regime where the ratio takes up the value $\sqrt{2}$. This intermediate saturation regime corresponds to the time scale $1/\gamma \ll t \ll L^2/D_{\mathrm{eff}}$ at which the dynamics of RTPs becomes effectively diffusive. The timescale at which the ratio saturates to 1 is the diffusive timescale which goes as $t \approx L^2/D$ for diffusive systems and $t \approx L^2/D_{\mathrm{eff}}$ for active systems, where D_{eff} is the effective diffusion constant for RTPs in one dimension.

Interestingly, we demonstrated that the boundary conditions also play a crucial role in determining the dynamic behavior of current fluctuations. The setup with two open boundaries displays larger fluctuations by a factor of 2 at short times compared to the setup with only one open boundary. However, the former setup exhibits lesser fluctuations by the same factor of 2 at large times. This can be qualitatively understood as follows: At short times, the particles in the setup with two open boundaries have two escape routes, thereby increasing the fluctuations by a factor of 2. However, at large times, the fluctuations are predominantly determined by single-particle events, and the probability that an unbiased single particle escapes through one of the boundaries is $1/2$. Consequently, this reduces the fluctuations by a factor of 2.

Our exact analytical results reveal how slight variations in the initial conditions and system geometry can affect the dynamic behavior of current fluctuations in stochastic systems. Our study is a first step towards understanding the effusion of particles through finite-sized regions across different spatial dimensions, which can be investigated using similar methods discussed in this paper. As previously mentioned the study of particle effusion has applications in designing membranes and porous materials, where controlled diffusion or leakage plays a pivotal role, as well as in the transportation of ions or molecules across cellular membranes [54–56]. Naturally, a careful analytical analysis of the problem of effusion through different confining volumes in higher dimensions will help to understand the underlying factors governing current fluctuations. For example, consider N particles starting their motion inside a d-dimensional hyper-cube. At large enough times, one would expect all the N particles to leave the cube which results in the mean being saturated to N whereas the variance approaches zero. Furthermore, as the annealed and quenched variances converge depending on the system size, higher dimensional diffusion should also exhibit the same behavior at very large enough times, beyond the system size-dependent timescale. However, we must emphasize that these are predictions inferred from the one-dimensional results. The problem of higher-dimensional diffusion is indeed an interesting and challenging topic, which could be explored in future works.

Note that throughout the article, we have considered the velocity of RTPs to be annealed. One could also quench the velocity degree of freedom of the RTPs and perform the same analysis. However, the primary reason we did not do so in the manuscript is as follows: Jose *et al* [38] demonstrates that when both the velocity and position are quenched simultaneously, the short-time behavior of the variance ($t \ll 1/\gamma$) exhibits a different power-law exponent compared to the case with annealed velocity and quenched position. In contrast, at sufficiently large times ($t \gg 1/\gamma$), the variances in both scenarios become exactly equal. In our analysis, we observed that finite-size effects in all the setups considered emerge on timescales of $L^2/D_{\text{eff}} \gg 1/\gamma$. At such large timescales, the results for quenched and annealed velocities (even with finite system size) converge. In summary, with the quenched velocity of RTPs, the short-time results would align with those in [38], while the large-time behavior would remain consistent with the current results.

It would be intriguing to investigate whether a universal behavior of current fluctuations exists, one that depends on the system's geometry, determined by factors such as the number of reflecting boundaries and available escape routes. Testing the results of this paper using coarse-grained field theories such as macroscopic fluctuation theory [57–63] is also a worthwhile future investigation. Finally, it would also be interesting to extend the computations presented in this paper to interacting systems such as the symmetric simple exclusion process [3, 64–67] and the ABC model [68, 69].

Data availability statement

All data that support the findings of this study are included within the article (and any supplementary files).

Acknowledgments

The numerical calculations reported in this work were carried out on the Nandadevi and Kamet cluster, which is maintained and supported by The Institute of Mathematical Science's High-Performance Computing Center. K R acknowledges funding through intramural funds at TIFR Hyderabad and the SERB-MATRICS Grant MTR/2022/000966. A P gratefully acknowledges research support from the Department of Science and Technology, India, SERB Start-up Research Grant Number SRG/2022/000080, and the Department of Atomic Energy, India.

Appendix A. Current fluctuations for Brownian particles confined in a finite interval—quenched setting

For a Brownian particle confined in a finite interval, the function $U(x_i,t)$ can be computed as in equation (43). In Laplace space, this expression becomes

$$\widetilde{U}(x_i,s) = \frac{\mathrm{e}^{-\sqrt{\frac{s}{D}}(L+x_i)}\left(1+\mathrm{e}^{\sqrt{\frac{s}{D}}(L+2x_i)}\right)}{2s}. \tag{A1}$$

The variance in the quenched setting can be computed by taking a Laplace transform of the expression in equation (27). This yields

$$\widetilde{\sigma}_{\mathrm{qu}}(L,s)^2 = \widetilde{\mu}_{\mathrm{qu}}(L,s) - \rho\int_0^L \mathrm{d}z\,\mathcal{L}(s)\left[U^2(z,t)\right]. \tag{A2}$$

The expression for $\widetilde{\mu}^{\mathrm{diff}}_{\mathrm{qu}}(L,s)$ for Brownian motion can be computed as

$$\widetilde{\mu}^{\mathrm{diff}}_{\mathrm{qu}}(L,s) = \rho\int_0^L \widetilde{U}(z,s)\,\mathrm{d}z = \rho\left(1-\mathrm{e}^{-L\sqrt{\frac{s}{D}}}\right)\sqrt{\frac{D}{s^3}}. \tag{A3}$$

The integral in the second term of equation (A2) can be computed using the identity

$$\int_0^L \mathrm{d}z\,\mathcal{L}(s)\left[U^2(z,t)\right] = \frac{1}{2\pi}\int_{-\infty}^{\infty}\mathrm{d}k\int_0^L \mathrm{d}z\,\widetilde{U}(z,s/2-ik)\,\widetilde{U}(z,s/2+ik). \tag{A4}$$

We provide a short derivation of this identity below,

$$\begin{aligned}
\int_0^L \mathrm{d}z\,\mathcal{L}(s)\left[U^2(z,t)\right] &= \int_0^L \mathrm{d}z\int_0^\infty \mathrm{d}t\mathrm{e}^{-st/2}U(z,t) \\
&\quad\times\int_0^\infty \mathrm{d}t'\delta(t-t')\,\mathrm{e}^{-st'/2}U(z,t') \\
&= \int_0^L \mathrm{d}z\int_0^\infty \mathrm{d}t\mathrm{e}^{-st/2}U(z,t) \\
&\quad\times\int_0^\infty \mathrm{d}t'\left(\frac{1}{2\pi}\int_{-\infty}^{\infty}\mathrm{d}k\mathrm{e}^{ik(t-t')}\right)\mathrm{e}^{-st'/2}U(z,t') \\
&= \frac{1}{2\pi}\int_{-\infty}^{\infty}\mathrm{d}k\int_0^L \mathrm{d}z\int_0^\infty \mathrm{d}t\mathrm{e}^{-st/2}\mathrm{e}^{ikt}U(z,t)
\end{aligned}$$

$$\times \int_0^\infty \mathrm{d}t' \mathrm{e}^{-st'/2} \mathrm{e}^{-ikt'} U(z,t')$$
$$= \frac{1}{2\pi} \int_{-\infty}^{\infty} \mathrm{d}k \int_0^L \mathrm{d}z\, \widetilde{U}(z, s/2 - ik)\, \widetilde{U}(z, s/2 + ik)\,. \tag{A5}$$

The integral over z in equation (A4) can be done explicitly. Since the resultant expression is quite long, we do not quote it here. However, this expression admits scaling forms in the limits, $s \to 0$ and $s \to \infty$. Let us denote

$$\widetilde{F}(k,s) = \int_0^L \mathrm{d}z\, \widetilde{U}(z, s/2 - ik)\, \widetilde{U}(z, s/2 + ik)\,. \tag{A6}$$

Using the substitution $u = k/s$, we obtain the following scaling forms for the function $\widetilde{F}(k,s)$,

$$\widetilde{F}(k,s) \xrightarrow[s\to 0]{} C_1(s)\, G_1(u)\,, \tag{A7}$$
$$\widetilde{F}(k,s) \xrightarrow[s\to \infty]{} C_2(s)\, G_2(u)\,, \tag{A8}$$

where

$$C_1(s) = \frac{L}{s^2} - \frac{L^2}{\sqrt{D} s^{3/2}}, \tag{A9}$$

and

$$C_2(s) = \frac{\sqrt{D}}{s^{5/2}}. \tag{A10}$$

The expression in equation (A4) can now be written as

$$\int_0^L \mathrm{d}z\, \mathcal{L}(s) \left[U^2(z,t)\right] = \frac{1}{2\pi} \int_{-\infty}^{\infty} \mathrm{d}k\, \widetilde{F}(k,s)$$
$$\xrightarrow[s\to 0]{} \frac{s\, C_1(s)}{2\pi} \int_{-\infty}^{\infty} \mathrm{d}u\, G_1(u)\,.$$
$$\xrightarrow[s\to \infty]{} \frac{s\, C_2(s)}{2\pi} \int_{-\infty}^{\infty} \mathrm{d}u\, G_2(u)\,. \tag{A11}$$

It can be shown that the values of the integrals $\int_{-\infty}^{\infty} \mathrm{d}u\, G_1(u)$ and $\int_{-\infty}^{\infty} \mathrm{d}u\, G_2(u)$ appearing in the above expressions are exactly equal to 2π and $\pi(2 - \sqrt{2})$ respectively. Finally, we obtain

$$\int_0^L \mathrm{d}z\, \mathcal{L}(s)\left[U^2(z,t)\right] \xrightarrow[s\to 0]{} s\, C_1(s)$$
$$= \frac{L}{s} - \frac{L^2}{\sqrt{sD}}, \tag{A12}$$

and

$$\int_0^L \mathrm{d}z\, \mathcal{L}(s)\left[U^2(z,t)\right] \xrightarrow[s\to 0]{} s\frac{\sqrt{2}-1}{2}\, C_2(s)$$
$$= \frac{2-\sqrt{2}}{2}\frac{\sqrt{D}}{s^{3/2}}. \tag{A13}$$

Using equation (A3), it can also be shown that

$$\widetilde{\mu}_{\mathrm{qu}}^{\mathrm{diff}}(L,s) \xrightarrow[s\to 0]{} \rho\left(\frac{L}{s} - \frac{L^2}{2\sqrt{sD}}\right), \tag{A14}$$
$$\widetilde{\mu}_{\mathrm{qu}}^{\mathrm{diff}}(L,s) \xrightarrow[s\to \infty]{} \frac{\rho\sqrt{D}}{s^{3/2}}. \tag{A15}$$

Combining results froms equations (A12) to (A14) in equation (A2), we obtain

$$\widetilde{\sigma}_{\mathrm{qu}}^{\mathrm{diff}}(L,s)^2 \xrightarrow[s\to 0]{} \rho\left(\frac{L}{s} - \frac{L^2}{2\sqrt{sD}}\right) - \rho\left(\frac{L}{s} - \frac{L^2}{\sqrt{sD}}\right)$$
$$= \frac{\rho L^2}{2\sqrt{sD}}, \tag{A16}$$

and

$$\widetilde{\sigma}_{\mathrm{qu}}^{\mathrm{diff}}(L,s)^2 \xrightarrow[s\to \infty]{} \rho\frac{\sqrt{D}}{s^{3/2}} - \rho\frac{2-\sqrt{2}}{2}\frac{\sqrt{D}}{s^{3/2}}$$
$$= \frac{\rho\sqrt{D}}{\sqrt{2}s^{3/2}}, \tag{A17}$$

which on inversion yield

$$\sigma_{\mathrm{qu}}^{\mathrm{diff}}(L,t)^2 \xrightarrow[t\to \infty]{} \frac{\rho L^2}{2\sqrt{\pi Dt}}, \tag{A18}$$

and

$$\sigma_{\mathrm{qu}}^{\mathrm{diff}}(L,t)^2 \xrightarrow[t\to 0]{} \sqrt{2}\frac{\rho\sqrt{Dt}}{\sqrt{\pi}}. \tag{A19}$$

The expression in equation (A18) is exactly equal to the large time asymptotic expression for the variance in the annealed setting we obtained previously in equation (46).

Appendix B. Current fluctuations for run and tumble particles confined in a finite interval—quenched setting

For a RTP confined in a finite interval, the function $\widetilde{U}(x_i, s)$ can be computed as in equation (66). Similar to the case for Brownian motion, the variance in the quenched setting can be computed using the expression in equation (A2). The exact expression for the mean in Laplace space $\widetilde{\mu}_{\rm qu}^{\rm rtp}(L,s)$, is given in equation (67). As for the Brownian case, the integral in the second term in equation (A2) can be computed using the identity given in equation (A4). After performing the integral over z, we obtain scaling forms of the resultant expression in the asymptotic limits, $s \to 0$ and $s \to \infty$. Using the substitution $u = k/s$, we obtain the following scaling forms for the function $\widetilde{F}(k,s)$ defined in equation (A6),

$$\widetilde{F}(k,s) \xrightarrow[s\to 0]{} C_1(s)\, G_1(u)\,, \tag{B1}$$

$$\widetilde{F}(k,s) \xrightarrow[s\to \infty]{} C_2(s)\, G_2(u)\,, \tag{B2}$$

where

$$C_1(s) = \frac{L}{s^2} - \frac{L^2}{\sqrt{D_{\rm eff}}\, s^{3/2}}, \tag{B3}$$

and

$$C_2(s) = \frac{v}{s^3}. \tag{B4}$$

Thus we obtain

$$\begin{aligned} \int_0^L \mathrm{d}z\, \mathcal{L}(s)\left[U^2(z,t)\right] &= \frac{1}{2\pi}\int_{-\infty}^{\infty} \mathrm{d}k\, \widetilde{F}(k,s) \\ &\xrightarrow[s\to 0]{} \frac{s\, C_1(s)}{2\pi}\int_{-\infty}^{\infty} \mathrm{d}u\, G_1(u)\,. \\ &\xrightarrow[s\to \infty]{} \frac{s\, C_2(s)}{2\pi}\int_{-\infty}^{\infty} \mathrm{d}u\, G_2(u)\,. \end{aligned} \tag{B5}$$

It can be shown that the values of the integrals $\int_{-\infty}^{\infty} \mathrm{d}u\, G_1(u)$ and $\int_{-\infty}^{\infty} \mathrm{d}u\, G_2(u)$ appearing in the above expressions are exactly equal to 2π and π respectively. Finally, we obtain

$$\begin{aligned} \int_0^L \mathrm{d}z\, \mathcal{L}(s)\left[U^2(z,t)\right] &\xrightarrow[s\to 0]{} s\, C_1(s) \\ &= \frac{L}{s} - \frac{L^2}{\sqrt{s D_{\rm eff}}}, \end{aligned} \tag{B6}$$

and

$$\begin{aligned} \int_0^L \mathrm{d}z\, \mathcal{L}(s)\left[U^2(z,t)\right] &\xrightarrow[s\to \infty]{} \frac{s}{4}\, C_2(s) \\ &= \frac{v}{2s^2}. \end{aligned} \tag{B7}$$

Using equation (67), it can also be shown that

$$\widetilde{\mu}_{\mathrm{qu}}^{\mathrm{rtp}}(L,s) \xrightarrow[s\to 0]{} \rho\left(\frac{L}{s}-\frac{L^2}{2\sqrt{sD_{\mathrm{eff}}}}\right), \tag{B8}$$

$$\widetilde{\mu}_{\mathrm{qu}}^{\mathrm{rtp}}(L,s) \xrightarrow[s\to \infty]{} \frac{\rho v}{s^2}. \tag{B9}$$

Combining results from equations (B6) to (B8) in equation (A2), we obtain

$$\begin{aligned}\widetilde{\sigma}_{\mathrm{qu}}^{\mathrm{rtp}}(L,s)^2 &\xrightarrow[s\to 0]{} \rho\left(\frac{L}{s}-\frac{L^2}{2\sqrt{sD_{\mathrm{eff}}}}\right)-\rho\left(\frac{L}{s}-\frac{L^2}{\sqrt{sD_{\mathrm{eff}}}}\right)\\ &= \frac{\rho L^2}{2\sqrt{sD_{\mathrm{eff}}}},\end{aligned} \tag{B10}$$

and

$$\begin{aligned}\widetilde{\sigma}_{\mathrm{qu}}^{\mathrm{rtp}}(L,s)^2 &\xrightarrow[s\to \infty]{} \rho\frac{v}{s^2}-\rho\frac{v}{2s^2}\\ &= \frac{\rho v}{2s^2},\end{aligned} \tag{B11}$$

which on inversion yield

$$\sigma_{\mathrm{qu}}^{\mathrm{rtp}}(L,t)^2 \xrightarrow[t\to \infty]{} \frac{\rho L^2}{2\sqrt{\pi D_{\mathrm{eff}} t}}, \tag{B12}$$

and

$$\sigma_{\mathrm{qu}}^{\mathrm{rtp}}(L,t)^2 \xrightarrow[t\to 0]{} \frac{\rho v t}{2}. \tag{B13}$$

The expression in equation (B12) is exactly equal to the large time asymptotic expression for the variance in the annealed setting we obtained previously in equation (69).

Appendix C. Details of numerical simulation

In this section, we provide details regarding the methods used for obtaining the numerical results for both the Brownian and RTP cases. In both these cases, we start with N number of particles uniformly distributed over the region $x \in [-L, 0]$. The resulting density of the number of particles is $\rho = N/L$. Thus the initial position of each particle i.e. x_i (where $i \in (1, N)$) can be generated by choosing a uniform random number from the interval $[-L, 0]$. The subsequent evolution of the systems are described below.

C.1. Brownian particles

To find the current we need to know the random position $X_i(t)$ of the ith particle at a time t. *In a single run* of the simulation, the final position $X_i(t)$ can be found by drawing a random number from the propagator of the underlying process. For the Brownian process in one-dimension with diffusion coefficient D the propagator is simply a Gaussian distribution given as [51]

$$G(x,t|x_i) = \frac{1}{\sqrt{4\pi D t}} \mathrm{e}^{-\frac{(x-x_i)^2}{4Dt}}. \tag{C1}$$

We draw a random number from this distribution at time t, to find $X_i(t)$.

For the open interval case, we calculate current $Q(t)$ for that particular run of the simulation by counting the number of particles for which $X_i(t)$ lies outside the interval $[-L, 0]$. However, in the presence of a reflecting boundary at $x = -L$ we use the reflection property of Brownian particles i.e. when the final position $X_i(t) < -L$ we reflect its position as $X_i(t) \to -2L - X_i(t)$ which bring its position above $x = -L$. In this case, $Q(t)$ is constructed out of particles that lie above the origin $x = 0$ at time t i.e. when $X_i(t) > 0$. The whole process is then repeated for a number of runs. The choice of initial conditions for each of the runs and the process of averaging out them is distinct in both the annealed and quenched settings as elaborated below.

Annealed case: in the annealed case for each of the runs, a completely different set of initial configurations $\{x_i\}$ of the particles are chosen. Finally, the averaging is performed over all of these runs. For example, if there are M number of runs then the mean and variance of the annealed current is found as

$$\langle Q \rangle_{\mathrm{an}} = \frac{1}{M} \sum_{j=1}^{M} Q_j, \text{ and } \sigma_{\mathrm{an}}^2 = \frac{1}{M} \sum_{j=1}^{M} Q_j^2 - \langle Q \rangle_{\mathrm{an}}^2, \tag{C2}$$

where Q_j is the current obtained from the jth run. In our simulations, we have used $M = 10^6$.

Quenched case: in the quenched case two-step averaging process is carried out. First, we chose one single set of random initial positions $\{x_i\}$. Then at each run the current Q is found and averaged over keeping the initial configurations fixed. Suppose, we do this for M_1 number of independent runs. If we denote the obtained average for the chosen fixed initial configuration by $\langle Q' \rangle$ then we have

$$\begin{aligned} \langle Q' \rangle_{\{x_i\}} &= \frac{1}{M_1} \sum_{j=1}^{M_1} Q_j, \\ \left(\sigma'_{\{x_i\}} \right)^2 &= \left(\frac{1}{M_1} \sum_{j=1}^{M_1} Q_j^2 \right) - \langle Q' \rangle_{\{x_i\}}^2, \end{aligned} \tag{C3}$$

where Q_j is the current obtained at the jth run for the particular initial configuration. Now, averaging is performed over Q' for different choices of the initial configurations. If there are M_2 number of such distinct initial configurations of the particles then the quenched average is found as

$$\langle Q \rangle_{\mathrm{qu}} = \frac{1}{M_2} \sum_{k=1}^{M_2} \langle Q' \rangle_k, \text{ and } \sigma_{\mathrm{qu}} = \frac{1}{M_2} \sum_{k=1}^{M_2} \left(\sigma'_k \right)^2, \tag{C4}$$

where we have denoted the quantities for different runs with the kth initial configuration by the subscript k. In our simulation, we have taken $M_1 = M_2 = 10^3$. Further, we have taken $D = 1$ and $\rho = 1$ (which also implies $N = L$) in both the annealed and quenched cases. Then the simulation is performed taking different values of L which are $10, 10^2$ and 10^3.

C.2. Run-and-tumble particles

For the run-tumble particles along with the initial positions of the particles, the initial velocity vector is also a random quantity. We deal with the case where the initial velocity $+v$ or $-v$

are chosen with equal probability $1/2$ for each of the particles. Now, each particle reverses its direction of propagation after a randomly distributed time τ, drawn from the exponential distribution $\gamma e^{-\gamma t}$. This motion is then continued up until the time t and the final position of the particle is noted. For the case with reflecting boundary if the particle crosses the boundary $x=-L$ at some intermediate time $t' \leqslant t$ then we again reflect its position $X_i(t')$ as $X_i(t') \to -2L - X_i(t')$.

The methods employed hereafter to find the annealed and quenched variances are exactly the same as discussed in the Brownian case. However, here the velocity was chosen randomly for each of the runs even with a fixed initial position as for the quenched case. Jose *et al* [38] discusses the cases (but for infinite system sizes) with annealed and quenched settings even for the random initial velocities. For averaging we have used $M = 10^5$ for the annealed case and $M_1 = 10^3$ and $M = 10^2$ for the quenched case (while these parameters are defined in the same way as in the Brownian case). In our simulation, we have chosen $v = \sqrt{0.2}, \gamma = 0.1$ so that $D_{\text{eff}} = v^2/2\gamma = 1$ for both the annealed and quenched cases.

Note that unlike the Brownian case here we do not take $\rho = 1$ for different values of L. Instead, we plot the rescaled (by the density ρ) mean and variance which are independent of ρ, as shown in figures 6 and 8. This is solely due to the time constraint on running the simulation with RTP. Evolving the RTP up to time $\mathcal{O}(10^7)$ consumes a substantial amount of time with the method described above. Thus keeping ρ fixed and increasing L increases the simulation time scale as $\propto \rho L$. To circumvent this issue we reduced the number of particles N while running the simulation for a larger value of L so that ρ is also reduced and thus the simulation time scale $\propto \rho L$ keeps unaltered even for higher L. As we see from the analytical expressions derived in the main text all the statistical properties of the current depend only linearly in ρ. Thus by rescaling the resulting quantity obtained from simulation by ρ we make sure no effect of ρ is present.

ORCID iDs

Arup Biswas https://orcid.org/0009-0007-5611-7709
Stephy Jose https://orcid.org/0000-0002-5089-9873
Arnab Pal https://orcid.org/0000-0001-6806-5431

References

[1] Le Doussal P and Machta J 1989 *Phys. Rev.* B **40** 9427
[2] Van Beijeren H 1991 *J. Stat. Phys.* **63** 47
[3] Derrida B, Douçot B and Roche P-E 2004 *J. Stat. Phys.* **115** 717
[4] Derrida B and Gerschenfeld A 2009 *J. Stat. Phys.* **137** 978
[5] Ferrari P L 2010 *J. Stat. Mech.* P10016
[6] Lizana L, Ambjörnsson T, Taloni A, Barkai E and Lomholt M A 2010 *Phys. Rev.* E **81** 051118
[7] Krapivsky P and Meerson B 2012 *Phys. Rev.* E **86** 031106
[8] Bodineau T and Derrida B 2004 *Phys. Rev. Lett.* **92** 180601
[9] Leibovich N and Barkai E 2013 *Phys. Rev.* E **88** 032107
[10] Krapivsky P, Mallick K and Sadhu T 2014 *Phys. Rev. Lett.* **113** 078101
[11] Banerjee T, Jack R L and Cates M E 2022 *Phys. Rev.* E **106** L062101
[12] Mallick K, Moriya H and Sasamoto T 2022 *Phys. Rev. Lett.* **129** 040601
[13] Dandekar R, Krapivsky P and Mallick K 2023 *Phys. Rev.* E **107** 044129
[14] Dean D S, Majumdar S N and Schehr G 2023 *J. Stat. Mech.* 063208
[15] Di Bello C, Hartmann A K, Majumdar S N, Mori F, Rosso A and Schehr G 2023 *Phys. Rev.* E **108** 014112
[16] Derrida B and Gerschenfeld A 2009 *J. Stat. Phys.* **136** 1

[17] Cividini J and Kundu A 2017 *J. Stat. Mech.* 083203
[18] Dagdug L, Pe na J and Pompa-García I 2024 *Diffusion Under Confinement: A Journey Through Counterintuition* (Springer) (https://doi.org/10.1007/978-3-031-46475-1)
[19] Fick A 1855 *Ann. Phys., Lpz.* **170** 59
[20] Jacobs M H 1935 *Diffusion Processes* (Springer) (https://doi.org/10.1007/978-3-642-86414-8_1)
[21] Zwanzig R 1992 *J. Phys. Chem.* **96** 3926
[22] Siwy Z and Fuliński A 2002 *Phys. Rev. Lett.* **89** 198103
[23] Siwy Z, Kosińska I, Fuliński A and Martin C 2005 *Phys. Rev. Lett.* **94** 048102
[24] Aksimentiev A, Heng J B, Timp G and Schulten K 2004 *Biophys. J.* **87** 2086
[25] Dagdug L, Berezhkovskii A M, Makhnovskii Y A and Zitserman V Y 2007 *J. Chem. Phys.* **127** 224712
[26] Jain S, Boyer D, Pal A and Dagdug L 2023 *J. Chem. Phys.* **158** 054113
[27] Berezhkovskii A M, Dagdug L and Bezrukov S M 2017 *J. Chem. Phys.* **147** 134104
[28] Rostovtseva T K, Sheldon K L, Hassanzadeh E, Monge C, Saks V, Bezrukov S M and Sackett D L 2008 *Proc. Natl Acad. Sci.* **105** 18746
[29] Hoogerheide D P, Gurnev P A, Rostovtseva T K and Bezrukov S M 2017 *Nanoscale* **9** 183
[30] Burada P S, Hänggi P, Marchesoni F, Schmid G and Talkner P 2009 *ChemPhysChem* **10** 45
[31] Burada P S, Schmid G, Talkner P, Hänggi P, Reguera D and Rubí J M 2008 *BioSystems* **93** 16
[32] Freyhardt C, Tsapatsis M, Lobo R, Balkus Jr K and Davis M 1996 *Nature* **381** 295
[33] Davis M E 2002 *Nature* **417** 813
[34] Fu J, Yoo J and Han J 2006 *Phys. Rev. Lett.* **97** 018103
[35] Keyser U, Van der Does J, Dekker C and Dekker N 2006 *Rev. Sci. Instrum.* **77** 105105
[36] Thorneywork A L, Gladrow J, Qing Y, Rico-Pasto M, Ritort F, Bayley H, Kolomeisky A B and Keyser U F 2020 *Sci. Adv.* **6** eaaz4642
[37] Banerjee T, Majumdar S N, Rosso A and Schehr G 2020 *Phys. Rev.* E **101** 052101
[38] Jose S, Rosso A and Ramola K 2023 *Phys. Rev.* E **108** L052601
[39] Jose S, Rosso A and Ramola K 2023 (arXiv:2310.16811)
[40] Malakar K, Jemseena V, Kundu A, Kumar K V, Sabhapandit S, Majumdar S N, Redner S and Dhar A 2018 *J. Stat. Mech.* 043215
[41] Evans M R and Majumdar S N 2018 *J. Phys. A: Math. Theor.* **51** 475003
[42] Mori F, Le Doussal P, Majumdar S N and Schehr G 2020 *Phys. Rev. Lett.* **124** 090603
[43] Mori F, Le Doussal P, Majumdar S N and Schehr G 2020 *Phys. Rev.* E **102** 042133
[44] Singh P and Kundu A 2019 *J. Stat. Mech.* 083205
[45] Angelani L, Di Leonardo R and Paoluzzi M 2014 *Eur. Phys. J.* E **37** 1
[46] Martens K, Angelani L, Di Leonardo R and Bocquet L 2012 *Eur. Phys. J.* E **35** 1
[47] Mori F, Le Doussal P, Majumdar S N and Schehr G 2021 *Phys. Rev.* E **103** 062134
[48] Jose S, Mandal D, Barma M and Ramola K 2022 *Phys. Rev.* E **105** 064103
[49] Jose S 2022 *J. Stat. Mech.* 113208
[50] Mallikarjun R and Pal A 2023 *Physica* A **622** 128821
[51] Feller W 1991 *An Introduction to Probability Theory and Its Applications* vol 81 (Wiley)
[52] Mejía-Monasterio C, Oshanin G and Schehr G 2011 *J. Stat. Mech.* P06022
[53] Angelani L 2023 *J. Phys. A: Math. Theor.* **56** 455003
[54] Kärger J 2008 *Adsorption and Diffusion* (Springer) p 329
[55] Post M F 1991 *Studies in Surface Science and Catalysis* vol 58 (Elsevier) pp 391–443
[56] Marbach S 2021 *J. Chem. Phys.* **154** 171101
[57] Bertini L, De Sole A, Gabrielli D, Jona-Lasinio G and Landim C 2005 *Phys. Rev. Lett.* **94** 030601
[58] Bertini L, Sole A D, Gabrielli D, Jona-Lasinio G and Landim C 2006 *J. Stat. Phys.* **123** 237
[59] Bertini L, De Sole A, Gabrielli D, Jona-Lasinio G and Landim C 2007 *J. Stat. Mech.* P07014
[60] Bertini L, De Sole A, Gabrielli D, Jona-Lasinio G and Landim C 2009 *J. Stat. Phys.* **135** 857
[61] Derrida B 2007 *J. Stat. Mech.* P07023
[62] Agranov T, Ro S, Kafri Y and Lecomte V 2023 *SciPost Phys.* **14** 045
[63] Jose S, Dandekar R and Ramola K 2023 *J. Stat. Mech.* 083208
[64] Levitt D G 1973 *Phys. Rev.* A **8** 3050
[65] Arratia R 1983 *Ann. Probab.* **11** 362
[66] Krapivsky P L, Mallick K and Sadhu T 2015 *J. Stat. Phys.* **160** 885
[67] Dandekar R and Mallick K 2022 *J. Phys. A: Math. Theor.* **55** 435001
[68] Clincy M, Derrida B and Evans M 2003 *Phys. Rev.* E **67** 066115
[69] Bodineau T and Derrida B 2011 *J. Stat. Phys.* **145** 745